DOI: 10.1002/((please add manuscript number))
Article type: Communication

Host-guest hybrid redox materials self-assembled from polyoxometalates and single-walled carbon nanotubes

Jack W. Jordan, Grace A. Lowe, Robert L. McSweeney, Craig T. Stoppiello, Rhys W. Lodge, Stephen T. Skowron, Johannes Biskupek, Graham A. Rance, Ute Kaiser, Darren A. Walsh,* Graham N. Newton,* Andrei N. Khlobystov*

J. W. Jordan, Dr. R. L. McSweeney, Dr. C. T. Stoppiello, Dr. R. W. Lodge, Dr. S. T. Skowron, Prof. A. N. Khlobystov
School of Chemistry, University of Nottingham, Nottingham NG7 2RD, UK.

G. A. Lowe, Dr. D. A. Walsh, Dr. G. N. Newton
GSK Carbon Neutral Laboratories for Sustainable Chemistry, University of Nottingham, Nottingham NG7 2TU, UK.

Dr. J. Biskupek, Prof. Dr. U. Kaiser
Electron Microscopy Group of Materials Science, Ulm University, 89081 Ulm, Germany.

Dr. G. A. Rance
Nanoscale and Microscale Research Centre, University of Nottingham, Nottingham, NG7 2RD, UK.

E-mail: darren.walsh@nottingham.ac.uk, graham.newton@nottingham.ac.uk,

andrei.khlobystov@nottingham.ac.uk

Keywords: carbon nanotubes, polyoxometalates, nanoconfinement, redox materials,

electrochemistry

The development of next-generation molecular-electronic, electrocatalytic, and energy-storage systems depends on the availability of robust materials in which molecular charge storage sites and conductive hosts are in intimate contact. We show here that electron transfer from single-walled carbon nanotubes (SWNTs) to polyoxometalate (POM) clusters results in the spontaneous formation of host-guest POM@SWNT redox-active hybrid materials. The SWNTs can conduct charge to and from the encapsulated guest

molecules, allowing electrical access to >90% of the encapsulated redox species. Furthermore, the SWNT hosts provide a physical barrier, protecting the POMs from chemical degradation during charging/discharging and facilitating efficient electron transfer throughout the composite, even in electrolytes that usually destroy POMs.

The development of advanced molecular materials for applications such as energy storage and molecular computing depends on the availability of robust, redox-active solid-state materials.[1] Polyoxometalates (POMs) are nanometer-sized clusters of early transition metal (Mo, W, V, Nb, Ta) oxides with well-defined compositions and structures and which can undergo multi-electron redox transitions,[2] rendering them promising nodes for molecular flash memory systems[3] and as the redox components in electrochemical energy-storage devices.[4] However, two major hurdles must be overcome to realize these opportunities: (i) fully-oxidized POMs are electrically-insulating, limiting the flow of charge to and from redox centers, and (ii) POMs are often chemically and electrochemically unstable, especially in alkaline media.

Immobilization of POMs onto high-surface-area, conductive substrates such as single-walled carbon nanotubes (SWNTs) can potentially improve the electrical addressability and stability of the redox centers. This has been achieved using covalent functionalization of SWNTs,[5] electrostatic binding of POMs to SWNTs *via* covalently-linked organic cations,[6] and non-covalent interactions mediated by the organic 'antenna' groups of functionalized POMs.[7] However, the conductivity of SWNTs is reduced by covalent modification of the sp^2 carbon framework and electrostatically-bound POMs can be relatively easily dislodged from the carbon surface.[8] A possible strategy for increasing the stability of POMs at SWNT interfaces is to immobilise the POMs *within* SWNTs, potentially protecting them from detachment and/or degradation. Individual hexanuclear $[W_6O_{19}]^{2-}$ Lindqvist anions have been encapsulated within double-walled carbon nanotubes by nano-extraction from ethanolic solutions. However, the work did not extend to an exploration of the electrochemical properties

of the hybrid materials.[9] The lack of further progress in this area may be due to the assumed incompatibility of highly-charged POMs with the hydrophobic interior of SWNTs, a perception that is supported by recent predictions of strong repulsive interactions between ionic guests and the cavities of SWNTs.[10] As such, most work has focused on encapsulating charge-neutral species such as salts,[11] metallic and non-metallic nanostructures,[12] and organic molecules,[13] within SWNTs.

In this contribution, we report a surprisingly simple and highly efficient method for immobilizing POMs within SWNTs. Our method requires no reagents other than pristine SWNTs and aqueous POM solutions, and results in durable POM@SWNT hybrids in which the redox centers are electrically addressable, even in alkaline electrolytes that usually destroy POMs. $[PW_{12}O_{40}]^{3-}\{W_{12}\}$ and $[P_2W_{18}O_{62}]^{6-}\{W_{18}\}$, both of which are about 1 nm wide, were encapsulated within arc-discharge SWNTs with uniform diameters of 1.4 nm.[14] Addition of SWNTs to aqueous solutions of $\{W_{12}\}$ and $\{W_{18}\}$ results in reduction of the POMs, as indicated by the dark blue coloration of the solution (Figure 1A) at the solid-liquid interface (reminiscent of the formation of "heteropoly blues").[15] A similar type of electron transfer from SWNTs to metal-polyiodide clusters has been demonstrated to stabilize electron-accepting molecules in SWNTs.[16] Electron density is transferred from the SWNTs to the POMs, resulting in the electrostatically-driven encapsulation of the negatively-charged POMs within the now positively-charged SWNTs. (Figure 1B,C) The close fit between the crystallographic dimensions of the POMs and the internal diameter of the SWNTs indicates that the POMs desolvate upon entry, providing an additional entropic driving force for encapsulation. Linear sweep voltammetry (LSV) of empty SWNTs shows that low currents flow at voltages corresponding to the energy of the SWNT band gap, and a high currents flow at voltages corresponding to the energies of the van Hove singularities.[17] The Fermi potential of the SWNTs (top level of the highest van Hove singularity in the valence band) is higher than those

of the POM LUMOs (estimated from solution-phase voltammetry of the POMs, Figure 3B&C), explaining the spontaneous electron transfer from the SWNTs to POMs (Figure 1B).[18]

High-resolution transmission electron microscopy (HRTEM) of the POM@SWNT hybrid confirms that virtually all SWNTs are filled with POMs (Figure 2J). Note that HRTEM exposure times were kept to a minimum to avoid sample degradation (Figure S1 and S2). The dark-contrast POMs in the TEM images are 1.0-1.8 nm wide, indicating that the POMs have different orientations within the SWNT cavities (Figure 2E and F), similar to their behavior on graphene.[19] Aberration-corrected HRTEM (AC-HRTEM) imaging of individual molecules shows W-W distances between 2.5 Å and 3 Å, and energy-dispersive X-ray (EDX) analysis gives W:O ratios of 1:4.3 and 1:3.6, for $\{W_{12}\}$@SWNT and $\{W_{18}\}$@SWNT respectively, with no significant potassium signal, which remain in solution during the nanotube filling process (Fig. 2G, H).

Thermogravimetric analysis (TGA) reveals that the average loadings of the POMs in the SWNTs are 11-16 wt. % and 11-30 wt. % for $\{W_{12}\}$@SWNT and $\{W_{18}\}$@SWNT, respectively (Figure S3), consistent with the HRTEM data (Figure 2J). The charge distribution within the composites was elucidated by Raman spectroscopy using an excitation wavelength of 660 nm (1.88 eV), in resonance with the SWNTs.[16] The G-band of the SWNT shifted positive by 5.5 cm^{-1} and 6.5 cm^{-1}, respectively, upon formation of $\{W_{12}\}$@SWNT and $\{W_{18}\}$@SWNT hybrid materials, confirming that electrons were donated from the SWNT to the POM guests (Figure 1B).[20] The shift of the G-band corresponds to charges of 0.017 and 0.020 hole/C-atom in $\{W_{12}\}$@SWNT and $\{W_{18}\}$@SWNT respectively,[21] in reasonable agreement with the microscopically-estimated stoichiometries (Figure 1D). Charge neutrality of the host-guest complexes negates the need for additional charge-balancing cations in the POM@SWNT systems, a conclusion supported by the absence of potassium signals from the EDX analysis and X-ray photoelectron spectra of $\{W_{18}\}$@SWNT (See SI).

Solution phase voltammetry of $\{W_{12}\}$ and $\{W_{18}\}$ (Figure 3A-C) is typical of that expected for these materials (see SI for details).[22] Cyclic voltammograms (CVs) of a POM@SWNT film immobilized on a glassy-carbon electrode (black lines in Figure 3B and 3C) show that the POMs remain electrochemically active when encapsulated within the SWNTs. The first two reductions of $\{W_{12}\}$ shift negatively by about 0.2 V upon encapsulation and ΔE_p decreases to about 10 mV at a scan rate of 100 mVs^{-1} (close to the value of 0 mV expected for a fully electrochemically reversible surface-confined redox couple; Figure S4 C,D).[23] Moreover, the peak currents for oxidation/reduction of $\{W_{18}\}$@SWNT and $\{W_{12}\}$@SWNT increase linearly as the voltammetric scan rate increases, confirming that the POMs are in intimate contact with the SWNT walls and directly wired to the glassy-carbon current collector. (Figure S4 A,B) Integration of the charge under the first reduction waves in the CVs of $\{W_{18}\}$@SWNT and $\{W_{12}\}$@SWNT gives surface concentrations, Γ, of 33 nmol cm^{-2} and 19 nmol cm^{-2}, respectively, indicating that 80-90 % of the immobilized POMs are electrochemically addressable. Γ is independent of the scan rate, and ΔE_p increases very little as the scan rate increases (Figure S4 C,D), indicating that electron transfer to/from the immobilized POMs is rapid. The charge passed during repeated reduction/oxidation of $\{W_{18}\}$@SWNT remains at 58% of the initial level after 1000 cycles (Figure 3D,F), while free $\{W_{18}\}$ completely loses activity after 1000 cycles under the same conditions (Figure 3F and S5). TEM analysis of $\{W_{18}\}$@SWNT after CV measurements clearly shows that most POMs remain encapsulated and intact even after 1000 charge-discharge cycles (Figure 3G). We also tested the (electro)chemical stability of the encapsulated POM@SWNT in aqueous NaOH (pH 13), an environment in which POMs are usually hydrolyzed and decompose readily. TEM analysis shows that the POMs remain intact within the SWNT after contact with the alkaline medium (Figure S6). Furthermore, CVs of $\{W_{12}\}$@SWNT recorded at pH 13 reveal two well-defined, reversible redox couples with ΔE_p = 17 mV and 0 mV (for the couples near −0.6 V and −0.4 V, respectively, Figure 3E). The redox couples remain visible after as many as 15 potential

cycles. In contrast, without the protection offered by the SWNTs, free $\{W_{12}\}$ and $\{W_{18}\}$ instantaneously decompose under the same conditions (Figure S7). Remarkably, the electrochemical signature of POM@SWNT that was eventually lost in alkaline media could be recovered by immersing the POM@SWNTs in an acidic medium (Figure S8), demonstrating that the POM is protected within the SWNT at pH 13.

In summary, we have discovered an effective method for driving the encapsulation of POMs within SWNTs. The encapsulation process occurs spontaneously and irreversibly at room temperature in water, driven by emergent coulombic forces between the anionic POMs and cationic nanotubes, and yields densely-filled POM@SWNT hybrid materials. The encapsulated POMs retain their redox properties, even in environments in which POMs cannot usually exist. The reagent-free redox-driven nanoconfinement of hydrophilic polyanionic materials within hydrophobic nanoscale carbon channels (which until now were considered incompatible) opens up new opportunities for the scalable and sustainable synthesis of hybrid functional materials from POMs combined with other types of porous carbons and other nanomaterials.

Supporting Information

Experimental details and additional characterization data are available from the Wiley Online Library or from the author.

Acknowledgements

JWJ, GAL, DAW, GNN, and ANK thank the EPSRC for funding through the Centre for Doctoral Training in Sustainable Chemistry (EP/L015633/1). DAW thanks the EPSRC for funding through project EP/P002382/1. U.K. and J.B. thank the DFG and the State Baden Württemberg for financial support in the frame of the SALVE project. ANK thanks the EPSRC (Established Career Fellowship). DAW and GNN thank the Advanced Molecular Materials

RPA and Propulsion Futures Beacon of Excellence within the University of Nottingham. The authors thank Dr. Emily Smith and Dr. Jesum Alves Fernandes for assistance with XPS measurements and discussion.

Received: ((will be filled in by the editorial staff))

Revised: ((will be filled in by the editorial staff))

Published online: ((will be filled in by the editorial staff))

References

[1] a) B. Dunn, H. Kamath, J.-M. Tarascon, *Science* **2011**, *334*, 928; b) Z. Liu, A. A. Yasseri, J. S. Lindsey, D. F. Bocian, *Science* **2003**, *302*, 1543; D. J. Wales, Q. Cao, K. Kastner, E. Karjalainen, G. N. Newton, V. Sans, *Adv. Mater.* **2018**, *30*, 1800159.

[2] D. L. Long, E. Burkholder, L. Cronin, *Chem. Soc. Rev.* **2007**, *36*, 105.

[3] C. Busche, L. Vilà-Nadal, J. Yan, H. N. Miras, D. L. Long, V. P. Georgiev, A. Asenov, R. H. Pedersen, N. Gadegaard, M. M. Mirza, D. J. Paul, J. M. Poblet, L. Cronin, *Nature* **2014**, *515*, 545.

[4] N. I. Gumerova, A. Rompel, *Nat. Rev. Chem.* **2018,** *2*, 0112.

[5] a) W. Chen, L. Huang, J. Hu, T. Li, F. Jia, Y. -F. Song, *Phys. Chem. Chem. Phys.* **2015**, 16, 19668; b) Y. Ji, L. Huang, J. Hu, C. Streb, Y. -F. Song, *Energy Environ. Sci.* **2015**, *8*, 776.

[6] F. M. Toma, A. Sartorel, M. Iurlo, M. Carraro, P. Parisse, C. Maccato, S. Rapino, B.Rodriguez Gonzalez, H. Amenitsch, T. Da Ros, L. Casalis, A. Goldoni, M. Marcaccio, G. Scorrano, G. Scoles, F. Paolucci, M. Prato, M. Bonchio, *Nat. Chem.* **2010**, *2*, 826.

[7] D. Ma, L. Liang, W. Chen, H. Liu, Y. -F. Song, *Adv. Funct. Mater.* **2013**, *23*, 6100.

[8] J. Hu, Y. Ji, W. Chen, C. Streb, Y. F. Song *Energy Environ. Sci.*, **2016**, 9, 1095.

[9] J. Sloan, G. Matthewman, C. Dyer-Smith, A. -Y. Sung, Z. Liu, K. Suenaga, A. I. Kirkland, E. Flahaut, *ACS Nano* **2008**, 2, 966.

[10] a) J. M. Wynn, P. V. C. Medeiros, A. Vasylenko, J. Sloan, D. Quigley, A. J. Morris *Phys. Rev. Materials* 2017, *1*, 073001(R); b) P. V. C. Medeiros, S. Marks, J. M. Wynn, A. Vasylenko, Q. M. Ramasse, D. Quigley, J. Sloan, A. J. Morris, *ACS Nano* 2017, *11*, 6178.

[11] R. R. Meyer, J. Sloan, R. E. Dunin-Borkowski, A. I. Kirkland, M. C. Novotny, S. R. Bailey, J. L. Hutchison, M. L. H. Green, *Science* **2000**, *289*, 1324.

[12] a) Z. Wang, K. Zhao, H. Li, Z. Liu, Z. Shi, J. Lu, K. Suenaga, S. -K. Joung, T. Okazaki, Z. Jin, Z. Gu, Z. Gao, S. Iijima, *J. Mater. Chem.* **2011**, 21, 171; b) Z. Wang, H. Li, Z. Liu, Z. Shi, J. Lu, K. Suenaga, S. -K. Joung, T. Okazaki, Z. Gu, J. Zhou, Z. Gao, G. Li, S. Sanvito, E. Wang, S. Iijima, *J. Am. Chem. Soc.* **2010**, *132*, 13840; c) T. W. Chamberlain, T. Zoberbier, J. Biskupek, A. Botos, U. Kaiser, A. N. Khlobystov, *Chem. Sci.* **2012**, *3*, 1919; d) T. Zoberbier, T. W. Chamberlain, J. Biskupek, N. Kuganathan, S. Eyhusen, E. Bichoutskaia, U. Kaiser, A. N. Khlobystov, *J. Am. Chem. Soc.* **2012**, *134*, 3073.

[13] S. T. Skowron, T. W. Chamberlain, J. Biskupek, U. Kaiser, E. Besley, A. N. Khlobystov, *Acc. Chem. Res.* **2017**, *50*, 1797.

[14] D. A. Britz, A. N. Khlobsytov, *Chem. Soc. Rev.* **35**, 637–659 (2006).

[15] M. T. Pope, G. M. Varga, *Inorg. Chem.* **1966**, *5*, 1249.

[16] A. Botos, J. Biskupek, T. W. Chamberlain, G. A. Rance, C. T. Stoppiello, J. Sloan, Z. Liu, K. Suenaga, U. Kaiser, A. N. Khlobystov, *J. Am. Chem. Soc.* **2016**, *138*, 8175.

[17] A. Al-zubaidi, T. Inoue, T. Matsushita, Y. Ishii, T. Hashimoto, S. Kawasaki, *J. Phys. Chem. C* **2012**, 116, 7681.

[18] R. L. McSweeney, T. W. Chamberlain, M. Baldoni, M. A. Lebedeva, E. S. Davies, E. Besley, A. N. Khlobystov, *Chem. Eur. J.* **2016**, 22, 13540.

[19] N. Vats, S. Rauschenbach, W. Sigle, S. Sen, S. Abb, A. Portz, M. Dürr, M. Burghard, P. A. van Aken, K. Kern, *Nanoscale* **2018**, *10*, 4952.

[20] a) H. Kataura, Y. Kumazawa, Y. Maniwa, I. Umezu, S. Suzuki, Y. Ohtsuka, Y. Achiba, *Synth. Met.* **1999**, *103*, 2555; b) M. V. Kharlamova, *Prog. Mater. Sci.* **2016**, *77*, 125.

[21] G. U. Sumanaseker, J. L. Allen, S. L. Fang, A. L. Loper, A. M. Rao, P. C. Eklund, *J. Phys. Chem. B* **1999**, *103*, 4292.

[22] M. Sadakane, E. Steckhan, *Chem. Rev.* **1998**, *98*, 219.

[23] A. J. Bard, L. R. Faulkner, Electrochemical Methods: Fundamental and Applications, 2nd ed., 2001., p. 591.

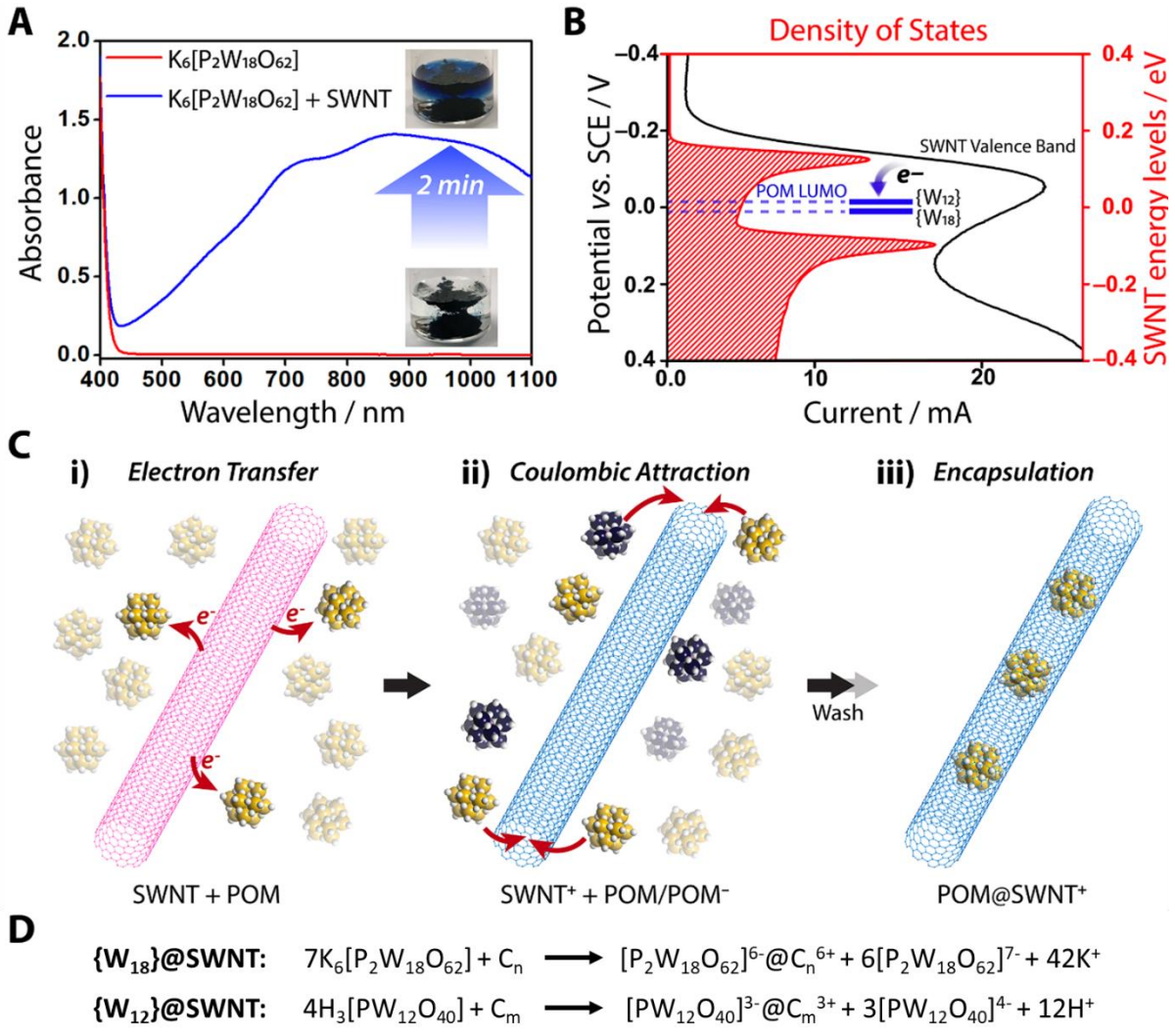

Figure 1. (A) UV-vis absorption spectrum of an aqueous solution of $K_6[P_2W_{18}O_{62}]$ before (red) and after contact with SWNTs (blue); (B) Electronic states of a (17,0) carbon nanotube (red plot), LUMO energy of POMs (blue, taken from CV in Figure 3B&C) and linear sweep voltammogram (LSV) of open, empty SWNTs (black plot); (C) Diagram showing (i) electron transfer from SWNTs (pink – neutral, blue – cationic) to POMs (yellow – native state, dark blue – reduced state); (ii) Columbic force-driven encapsulation of POM anions into the oxidized cationic SWNTs; (iii) Non-encapsulated POMs anions and all potassium cations are washed away using water. (D) Balanced equations of the redox reactions between POMs and nanotubes based on integration of TEM, Raman, EDX, TGA and XPS analytical data, where n = 420 and m = 530 are the estimated numbers of carbon atoms of the nanotube per encapsulated POM molecule.

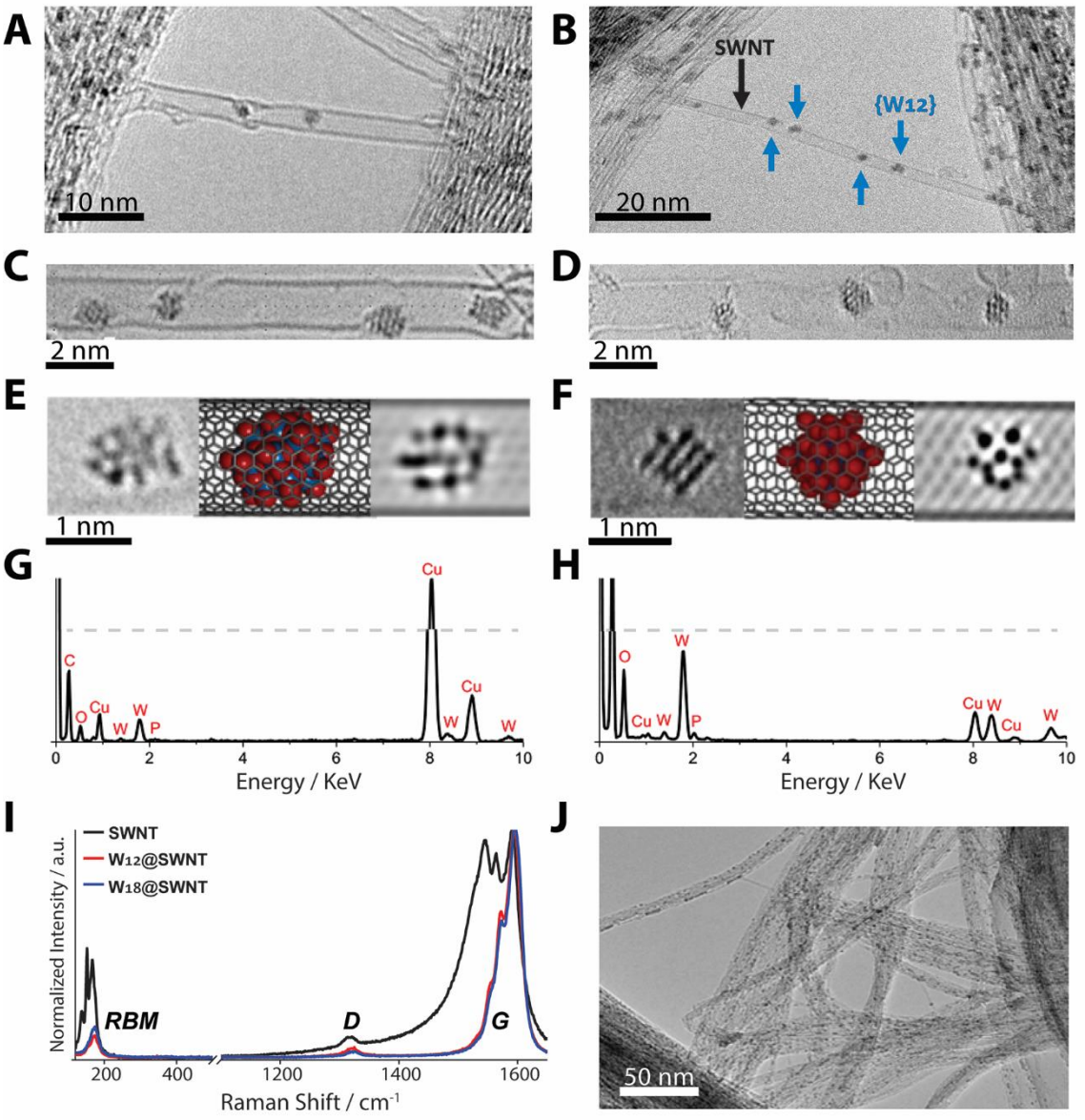

Figure 2. (A,B) HRTEM images of $\{W_{18}\}$@SWNT and $\{W_{12}\}$@SWNT respectively; (C, D) AC-HRTEM images of $\{W_{18}\}$@SWNT and $\{W_{12}\}$@SWNT; (E, F) Experimental TEM images, molecular models, and simulated images of single $\{W_{18}\}$ and $\{W_{12}\}$ POMs, respectively, in SWNTs. (G, H) EDX spectra of $\{W_{18}\}$@SWNT and $\{W_{12}\}$@SWNT, respectively. (I) Raman spectra of SWNTs, $\{W_{18}\}$@SWNT, and $\{W_{12}\}$@SWNT, showing the radial-breathing mode (RBM), D, and G bands. (J) Low-magnification TEM image of $\{W_{18}\}$@SWNT.

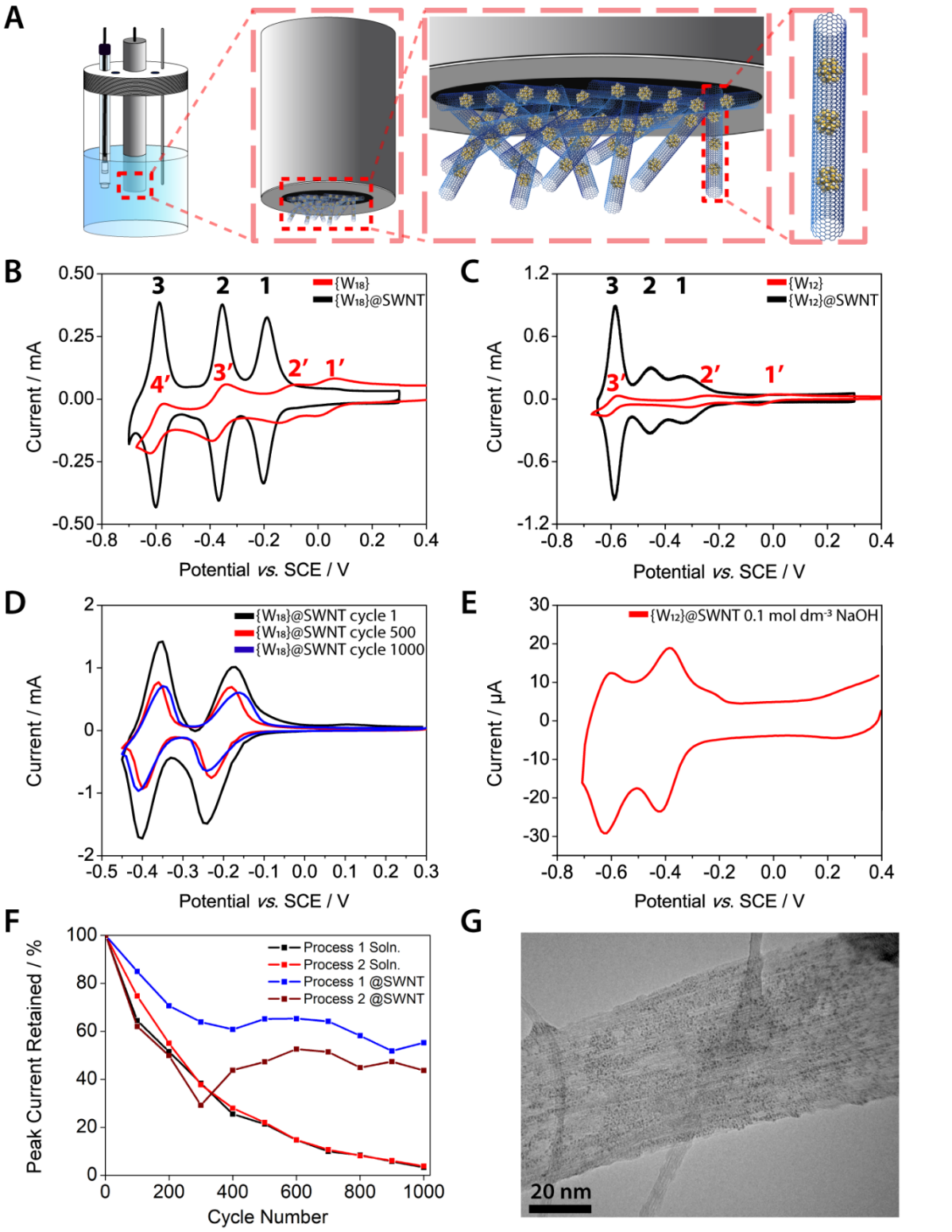

Figure 3. (A) Schematic of electrochemical cell used in our study; (B,C) Voltammograms of immobilized $\{W_{18}\}$@SWNT and $\{W_{12}\}$@SWNT, films respectively (black lines). The red lines show voltammograms of 5.0 mmol dm^{-3} $K_6\{W_{18}\}$ and $H_3\{W_{12}\}$, respectively, recorded

at a glassy-carbon working electrode. (D) 1st (black), 500th (red), and 1000th (blue) voltammograms of immobilized {W_{18}}@SWNT. All voltammograms were recorded at 100 mVs^{-1} in 1.0 mol dm^{-3} aqueous H_2SO_4. (E) Voltammogram of immobilized {W_{12}}@SWNT recorded at 100 mVs^{-1} in 0.1 mol dm^{-3} aqueous NaOH. (F) Changes in peak currents for molecules encapsulated inside nanotubes (blue and brown plots) and in solution (red and black plots). (G) TEM image of a large bundle of nanotubes in the {W_{18}}@SWNT sample after 1000 electrochemical cycles.

The reagent-free redox-driven nanoconfinement of polyoxometalate clusters within single-walled carbon nanotubes is demonstrated. The densely-packed chains of POM anions within cationic SWNTs form spontaneously and irreversibly under ambient conditions. Protected from the external environment and effectively ‘wired’ to the carbon support, the nanoconfined redox-active POMs exhibit exceptional electrochemical stability, even in environments in which they cannot usually exist.

Carbon nanotubes, polyoxometalates, nanoconfinement, redox materials, electrochemistry

Jack W. Jordan, Grace A. Lowe, Robert L. McSweeney, Craig T. Stoppiello, Rhys W. Lodge, Stephen T. Skowron, Johannes Biskupek, Graham A. Rance, Ute Kaiser, Darren A. Walsh,* Graham N. Newton,* Andrei N. Khlobystov*

Host-guest hybrid redox materials self-assembled from polyoxometalates and single-walled carbon nanotubes

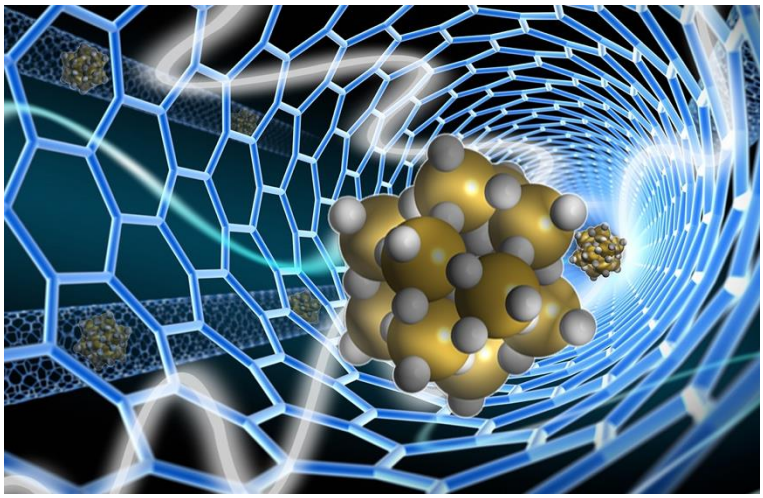

Supporting Information

Host-guest hybrid redox materials self-assembled from polyoxometalates and single-walled carbon nanotubes

Jack W. Jordan,[1] Grace A. Lowe,[2] Robert L. McSweeney,[1] Craig T. Stoppiello,[1] Rhys W. Lodge,[1] Stephen T. Skowron,[1] Johannes Biskupek,[3] Graham A. Rance,[4] Ute Kaiser,[3] Darren A. Walsh,[2] Graham N. Newton,[2*] Andrei N. Khlobystov[1*].*

[1] School of Chemistry, University of Nottingham, Nottingham NG7 2RD, UK.

[2] GSK Carbon Neutral Laboratories for Sustainable Chemistry, University of Nottingham, Nottingham NG7 2TU, UK.

[3] Electron Microscopy Group of Materials Science, Ulm University, 89081 Ulm, Germany.

[4] Nanoscale and Microscale Research Centre, University of Nottingham, Nottingham, NG7 2RD, UK.

Methods

Materials Preparation

$\{W_{12}\}$ and $\{W_{18}\}$ were synthesized using methods based on those reported in the literature.[1,2] A typical synthesis of POM@SWNT composite materials involved heating SWNTs (20 mg) at 600 °C for 30 minutes in order to remove the SWNT tips to allow molecules access to the SWNT cavity, as well as to remove adsorbates such as water and oxygen. The resulting black solid (10 mg) was then added to a rapidly stirred solution of POM (200 mg) in water (3 mL). The suspension was then sonicated for 2 minutes and subsequently stirred at room temperature for 2 days. The suspension was then filtered to give a black solid.

Raman Spectroscopy

Micro-Raman spectroscopy was performed using a Horiba-Jobin-Yvon LabRAM HR spectrometer. Single-point spectra were recorded using a 100× objective, a 300-μm confocal pinhole, and a 660 nm (1.88 eV) laser at < 0.3 mW. To simultaneously scan a range of Raman shifts, a 600-lines mm^{-1} rotatable diffraction grating was used. The spectral resolution was better than 1.2 cm^{-1}. Spectra were detected using a Synapse CCD detector (1024 pixels) thermoelectrically cooled to −60 °C. Instrument calibration was performed using the zero-order line and a standard Si(100) reference band at 520.7 cm^{-1}. Samples were prepared by depositing a small quantity of sample from a methanolic suspension onto Si(100) wafers, before drying under a stream of dry N_2. A typical spectrum was recorded by averaging 4-8 acquisitions, each of 5-30 s duration.

Transmission Electron Microscopy

Samples for transmission electron microscopy (TEM) were prepared by ultrasonically dispersing POM@SWNTs in propan-2-ol. Samples were drop cast onto lacey carbon-coated copper TEM grids. TEM images were recorded using a JEOL 2100 FEG-TEM microscope

operated at 100 kV. AC-HRTEM was performed at the University of Ulm on a C_s corrected FEI Titan 80-300 TEM operated at 80 kV with information-limit enhancement using reduced extraction voltage. Local EDX spectra were acquired for samples mounted on TEM grids using an Oxford Instruments INCA X-ray microanalysis system. The electron beam was condensed onto areas of specimens suspended over holes of the amorphous film. The experimental TEM images were accompanied by image simulation to confirm the findings. Structure models of POMs were embedded into models of SWNTs (chirality of the tubes was determined from the experimental images). The image simulation was carried out using the program QSTEM (www.qstem.org) that uses the multi-slice approach. Simulation parameters were the following: electron voltage U = 80 kV, slice thickness 0.1 nm/slice, spherical aberration C_s = 10 µm, focus ~ –6 nm (around Scherzerfocus, negative atoms contrast), focus spread Δf_s = 4 nm, convergence angle α = 0.1 mrad.

Thermal Analysis

Thermogravimetric analysis (TGA) was performed using a TA Q500 analyser. All samples were heated in Pt pans in air at a flow rate of 90 mL/min from room temperature to 1000 °C at ramp rate of 5 °C min^{-1} , and were then held at 1000 °C for 20 min.

Electrochemical Analysis

Electrochemical measurements were performed using a model CHI1140C potentiostat/galvanostat (CH Instruments, Austin, TX). A three-electrode electrochemical cell containing a 3 mm diameter glassy carbon (GC) disk working electrode, a Pt-wire counter electrode, and a saturated calomel reference electrode was used for all electrochemical measurements. Prior to use, the GC electrode was polished using aqueous suspensions of 1.0 µm, 0.3 µm, and 0.05 µm alumina (Buehler, Lake Bluff, Illinois) on felt polishing pads. The electrode was then rinsed thoroughly with deionized H_2O and dried. 1 wt.% suspensions of the

POM@SWNT containing 3 wt.% polytetrafluoroethylene binder were formed using ultrasonic agitation for 25 min. POM/SWNT films were formed on electrode surfaces by depositing 8 μL of the aqueous POM@SWNT suspension on the surface of the electrode. The electrochemical cell was charged with 5 mL of 1.0 mol dm^{-3} H_2SO_4 or 0.1 mol dm^{-3} NaOH, which had been purged of air with Ar for at least 15 min. A blanket of Ar was kept above the electrolyte during all measurements and the cell was kept at 25 °C by immersing the entire electrochemical cell into a temperature-controlled water bath. The effective concentration, Γ, of the immobilized POMs was determined using the equation $\Gamma = Q/n\mathrm{F}A$, where Q is the charge passed during reduction of the POMs, F is the Faraday constant, and A is the area of the electrode.

Modification of POMs under the Electron Beam

Aberration corrected high-resolution transmission electron microscopy (AC-HRTEM) allows the imaging of individual POMs with atomic resolution (Figure S1) and to follow processes of POM degradation and polycondensation in SWNTs directly at the single-molecule level, induced by the electron beam. Both samples showed cutting of the SWNTs and condensation of multiple POM molecules. The fragmentation and recombination witnessed leads to a variance in the sizes of the POM clusters observed during imaging, and the size distribution reported.

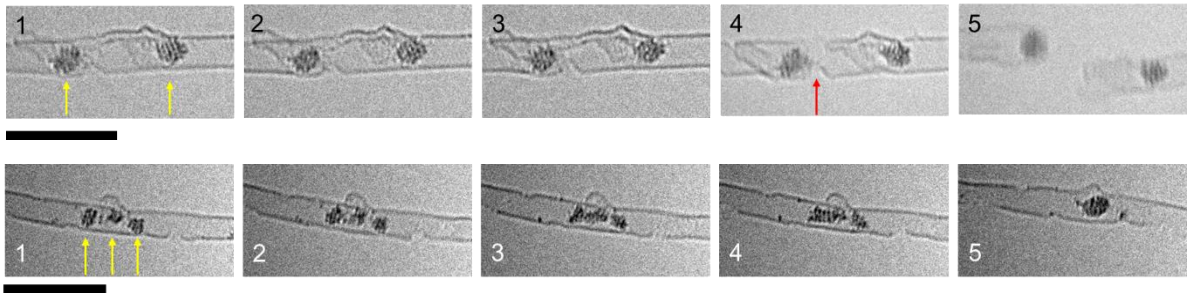

Figure S1. Time resolved AC-TEM images showing SWNT cutting (top) and polycondensation of multiple POM molecules in the $\{W_{18}\}$@SWNT sample, under the influence of the electron beam. Images acquired at 80 kV. Scale bars are 5 nm.

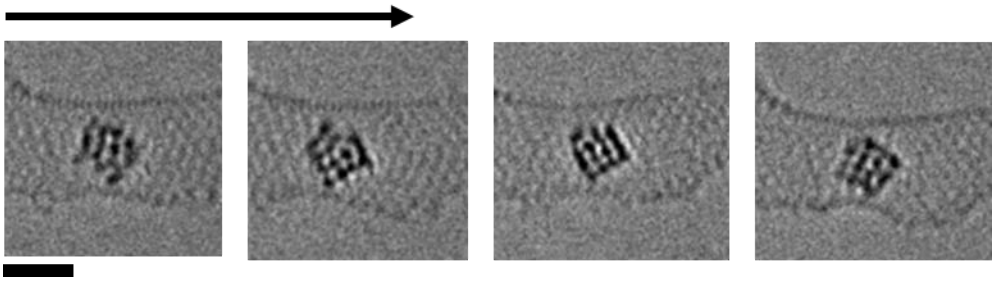

Figure S2. AC-TEM series of $\{W_{12}\}$@SWNT showing rotational and translational movement of a single POM within the SWNT interior over the course of 30 seconds. Images acquired at 80 kV. Scale bar is 1 nm.

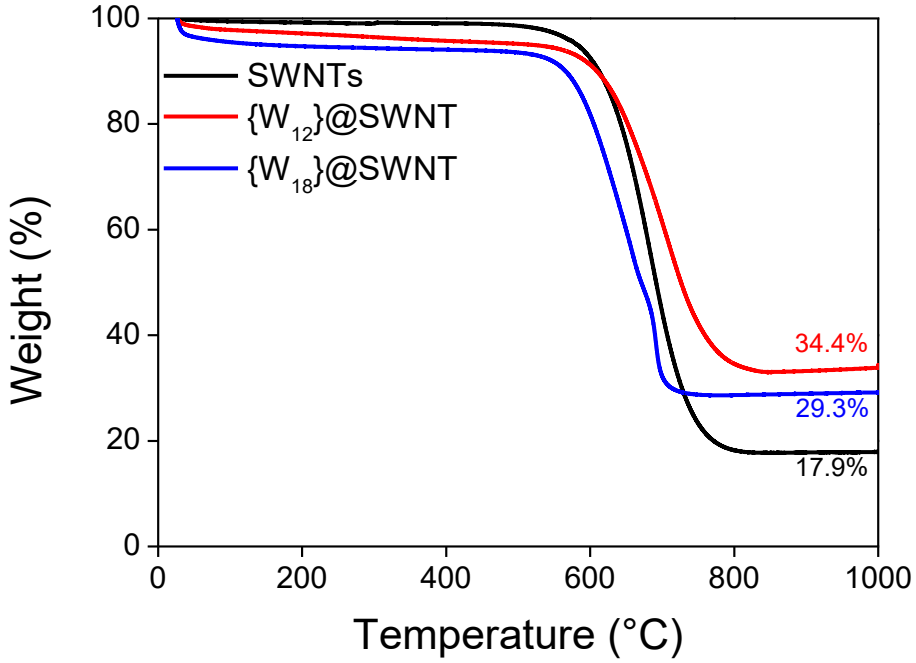

Figure S3. Thermal gravimetric analysis of the SWNTs, $\{W_{12}\}$@SWNT and $\{W_{18}\}$@SWNT samples, indicating the weight % loading of the redox-active POMs in the SWNTs.

Solution phase electrochemistry of {W_{12}} and {W_{18}} (see Figure 3A,B main manuscript). Four redox couples, with mid-point potentials of 0.03, −0.12, −0.37, and −0.60 V, and peak-to-peak separations, ΔE_p, of 48, 46, 46, and 37 mV, respectively, are observed, corresponding to two consecutive 1-electron processes followed by two 2-electron processes).[3] The CV of {W_{12}} dissolved in aqueous H_2SO_4 (red line in Figure 3B) shows 3 redox waves, with mid-point potentials of −0.02, −0.28, and −0.6 V, and ΔE_p values of 50, 56 and 32 mV, corresponding to two consecutive 1-electron processes, followed by a 2-electron process.[3]

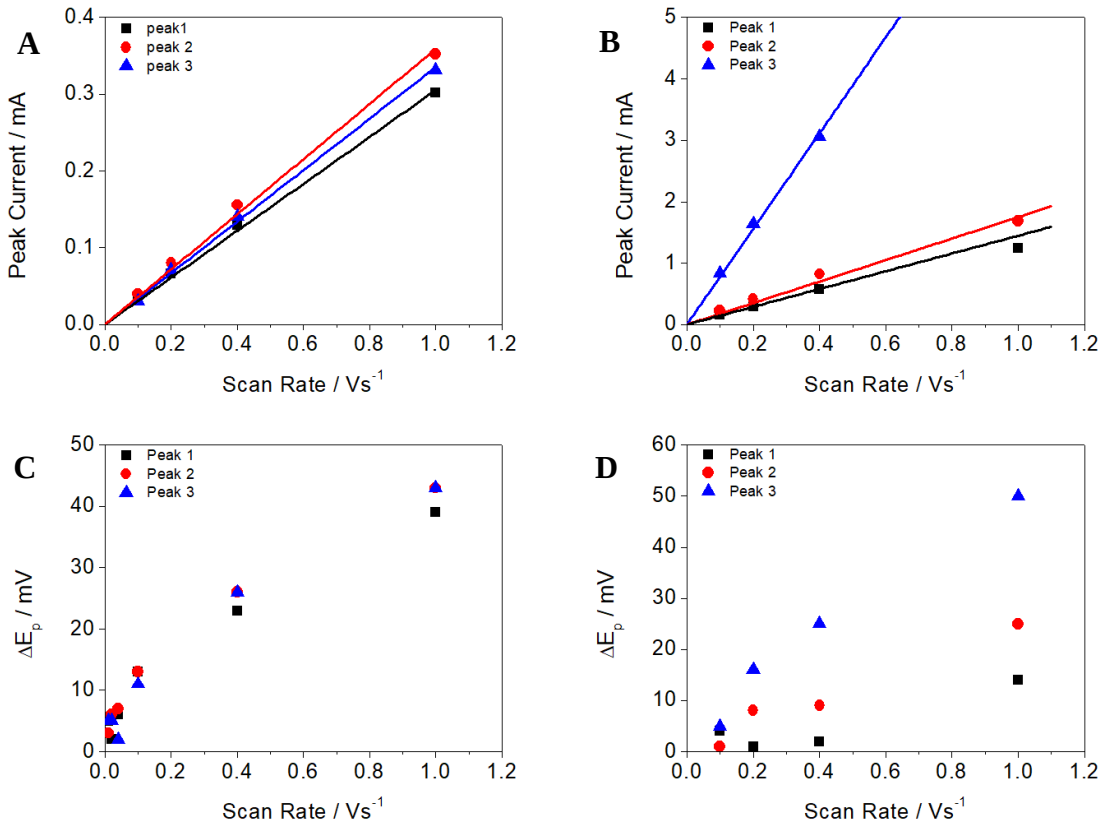

Figure S4. A and **B** show scan rate versus peak current for the oxidative waves for {W_{18}}@SWNT and {W_{12}}@SWNT respectively. **C** and **D** show peak to peak separation, ΔE_p, versus scan rate for {W_{18}}@SWNT and {W_{12}}@SWNT respectively.

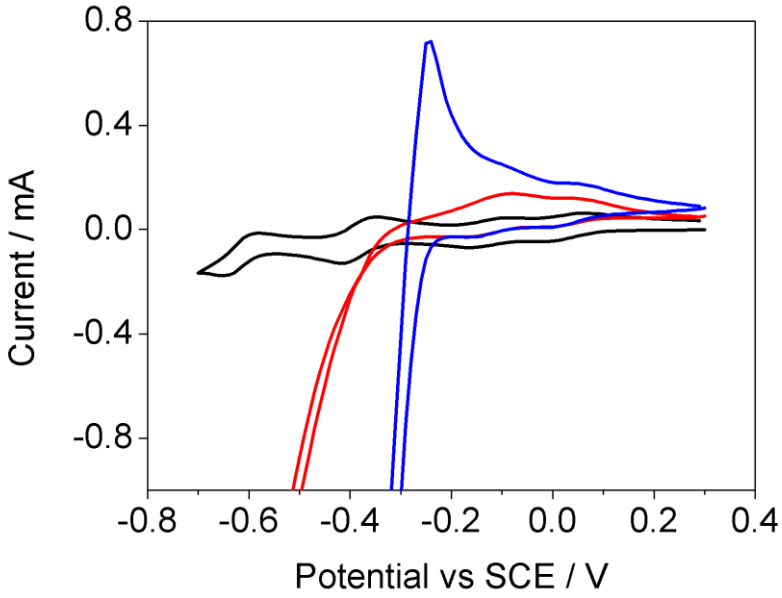

Figure S5. Cyclic voltammograms of $H_6[P_2W_{18}O_{62}]$ (5 mmol dm^{-3}) in 1 mol dm^{-3} H_2SO_4 at a glassy carbon working electrode. The 1st (black), 500th(red) and 1000th (blue) scans are shown.

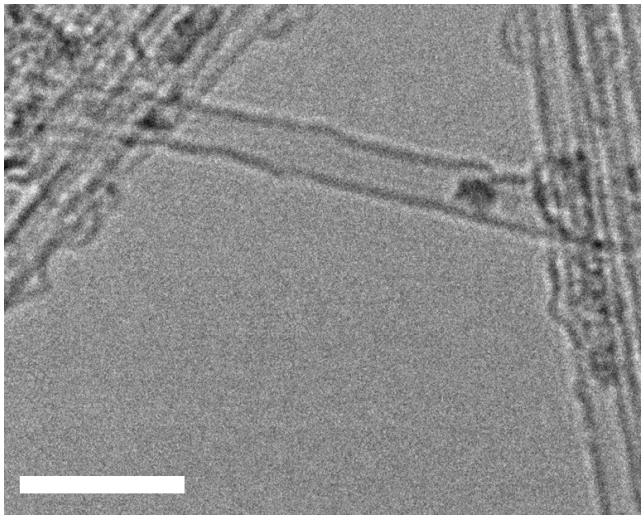

Figure S6. HRTEM image of $\{W_{18}\}$@SWNT sample after washing with base. The image shows that discrete structures persist. Image acquired at 100 kV. Scale bar is 5 nm.

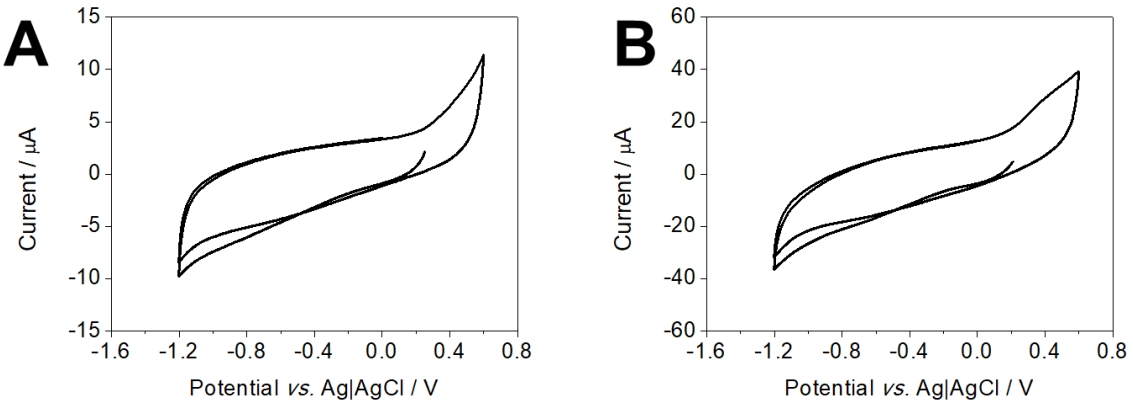

Figure S7. (A) Electrochemical response of $K_6[P_2W_{18}O_{62}]$ in 1M NaOH and **(B)** electrochemical response of $H_3[PW_{12}O_{40}]$ in 1M NaOH, with neither showing any redox processes.

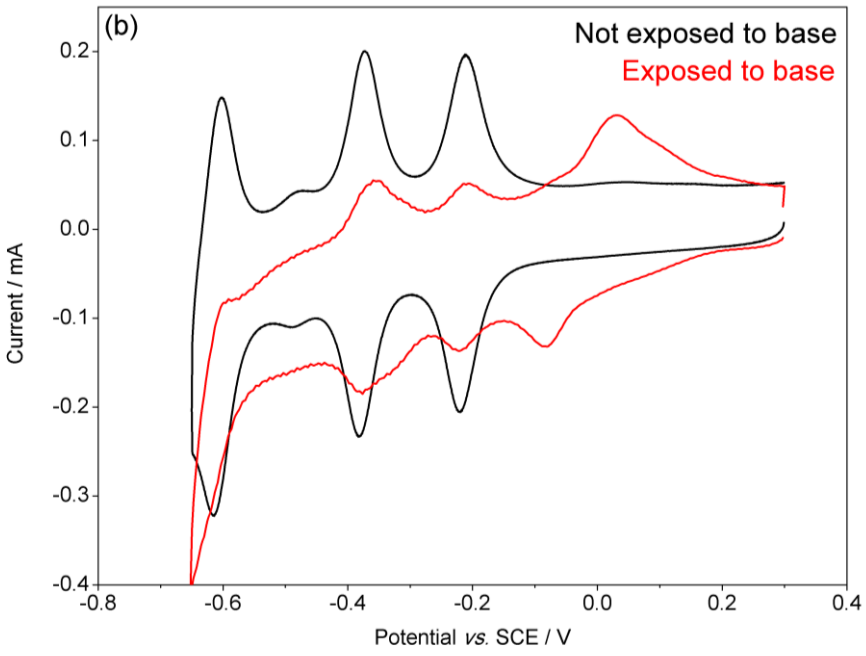

Figure S8. Electrochemical response of $\{W_{18}\}$@SWNT in 1M H_2SO_4 at 100 mV s^{-1} before 15 potential cycles in 1M NaOH (black) and after cycling 1M NaOH (red).

Raman spectroscopy

Earlier studies where the G-band shift was correlated with the number of electrons/holes transferred per carbon atom based on electrochemistry measurements reported a value of 320 cm^{-1} per unit of charge per C-atom as a quantitative measure of charge transfer.[4] This would equate to values of 0.017 and 0.020 electrons per C-atom donated from SWNT to $\{W_{12}\}$ and $\{W_{18}\}$, respectively. Based on the average separations between POM molecules in nanotubes of 3.9 nm and 3.1 nm observed by TEM for $\{W_{12}\}$ and $\{W_{18}\}$ in SWNT, respectively, the stoichiometry of $\{W_{12}\}$@SWNT and $\{W_{18}\}$@SWNT materials can be approximated as $[PW_{12}O_{40}]@C_{530}$ and $[P_2W_{18}O_{62}]@C_{420}$. Considering the charges on POMs and the charge-neutrality requirement, the formulae can be expressed as $[PW_{12}O_{40}]^{3-}@C_{530}^{3+}$ and $[P_2W_{18}O_{62}]^{6-}@C_{420}^{6+}$ with the amount of charge per C-atom of 0.006 e and 0.014 e lower but matching the trend observed in the G-band shift in Raman measurements for $\{W_{12}\}$@SWNT, and $\{W_{18}\}$@SWNT respectively. Considering the fact that both the spectroscopy (Raman) and direct space imaging (TEM) give the same order of magnitude for estimated charge on nanotube, and a clear correlation, the agreement between such fundamentally different methods of analysis is rather remarkable particularly for a heterogeneous/non-stoichiometric material.

Additionally, the changing shape of the G-band profile indicates that the SWNTs likely changed from metallic to semiconducting, due to band-gap opening upon charge transfer from the SWNTs to the POMs. The blue shifts in the SWNT radial breathing modes (RBMs) upon encapsulation confirm that the POMs were inside the SWNTs. Furthermore, the shift for $\{W_{18}\}$@SWNT (5.5 cm^{-1}) was larger than for $\{W_{12}\}$@SWNT (3.8 cm^{-1}), indicating that the interactions between the POMs and the carbon surface were stronger when the guest has a closer geometrical fit to the host.

X-Ray Photoelectron Spectroscopy (XPS)

XPS spectra of the free POM $K_6[P_2W_{18}O_{62}]$, empty SWNT and $\{W_{18}\}$@SWNT have been recorded and compared under the same experimental conditions (Figure S9). The atomic percent of elements estimated from 3 wide-scans for the free POM is close to the theoretical ratio of elements W:O = 1:2.8 and W:K = 3:1 in $K_6W_{18}PO_{62}$. A similar measurement for $\{W_{18}\}$@SWNT showed that the ratio of W:O remains unchanged as compared to the free POM, but K is absent, which is consistent with EDX and Raman measurements, and serves as another piece of evidence that the host-nanotube acts as a cation balancing the charge of the POM anion $[P_2W_{18}O_{62}]^{6-}$@$SWNT^{6+}$.

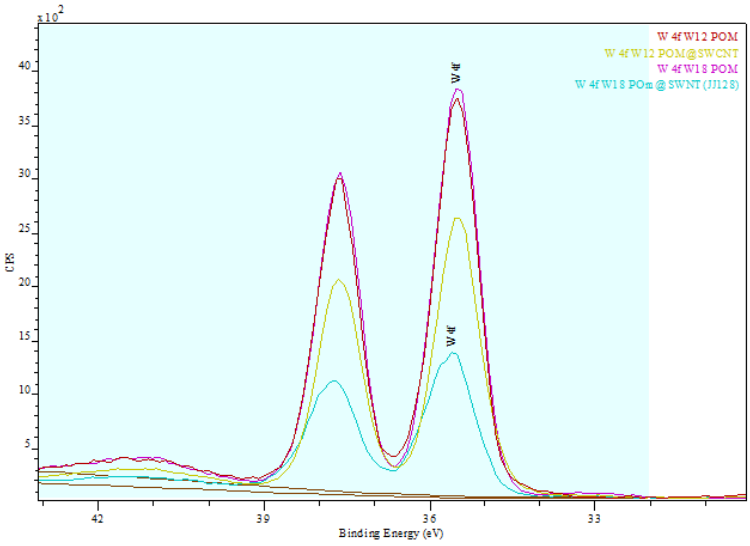

Figure S9. XPS spectra showing W 4f peaks for free POM $\{W_{18}\}$ (magenta) and $\{W_{18}\}$@SWNT (blue) overlaid with reference samples (red and yellow).

A close inspection of the position and shape of W 4f peak shows no measurable difference in the oxidation state of tungsten in $\{W_{18}\}$@SWNT as compared to free POM, consistent with the proposed mechanism of nanotube filling, and indicating that external POM molecules in solution act as oxidants inducing positive charge on SWNT (Figure 1B, main text).

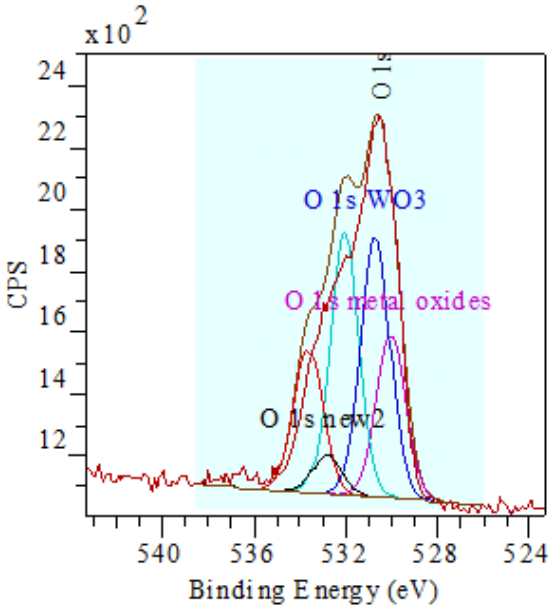

Figure S10. Peak fitting of an XPS spectrum of O 1s peaks {W_{18}}@SWNT.

Analysis and peak fitting of the shape of the O 1s peak (Figure S10) shows a complex overlap of different types of oxygen atoms, consistent with the different types of oxygen groups in the POM and a small percentage of oxygen present at SWNT defect sites.

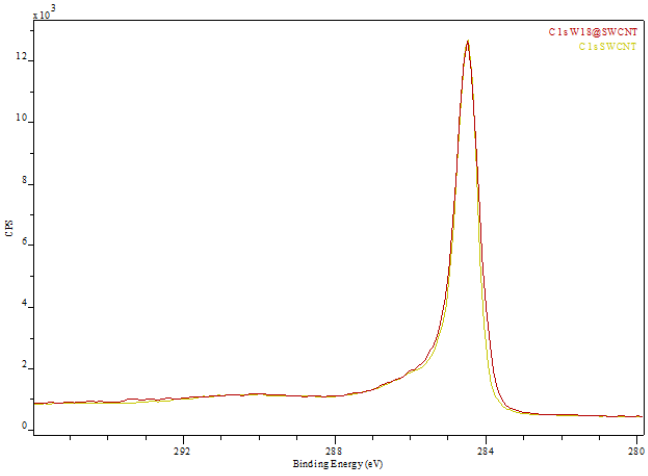

Figure S11. XPS spectra of C 1s peaks of empty SWNT (green) and {W_{18}}@SWNT (red).

The peak position and shape of the C 1s peaks (Figure S11) in empty nanotubes and nanotubes filled with the POM ({W_{18}}@SWNT) are virtually identical, indicating no chemical change in the host-nanotube upon encapsulation of the guest-POM.

Effect of chemisorbed O_2 on the Fermi level of SWNTs

If the synthesis of the POM-SWNT material was carried out using SWNTs that had been opened and exposed to air for a week, the formation of the blue solution at the solid liquid interface was not observed. This was hypothesized to be due to the Fermi level of the SWNTs decreasing in energy due to chemisorbed O_2 molecules which are removed from the SWNT sample during the annealing process. In order to test this hypothesis, a series of computational studies were carried out.

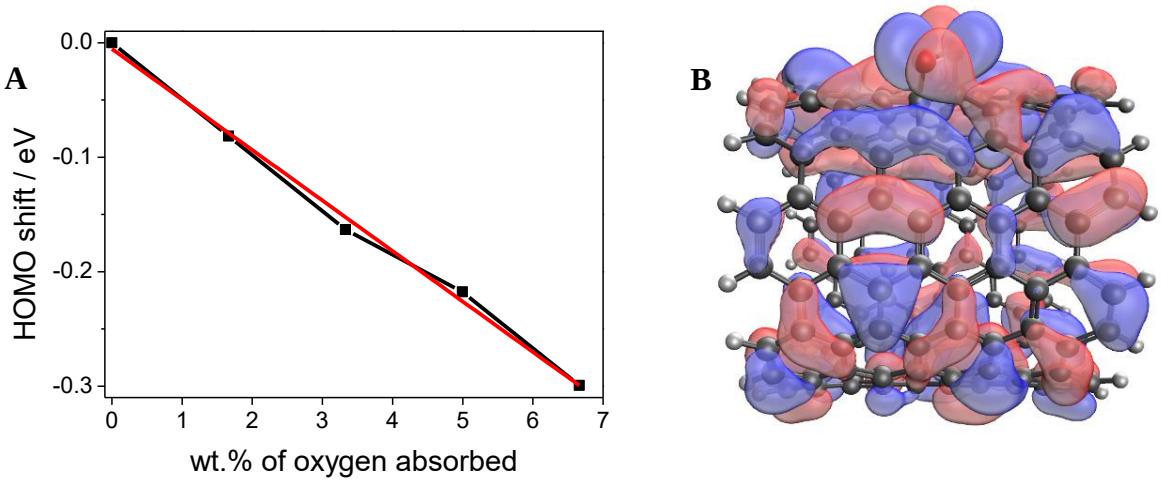

Figure S12. A shows the linear fit between an increasing weight percent of chemisorbed O_2 and a lowering of the HOMO energy in the model nanotube (equivalent of the Fermi level in SWNT sample). **B** illustrates the HOMO-8 orbital of the simulated system, clearly showing the oxygen molecule involved in bonding.

Our density functional theory calculations show that O_2 chemisorbs to the outside wall of the SWNT in the peroxide-like configuration (Figure S12), in agreement with previous theoretical results.[5] This binding mode decreases the energy of the HOMO of the system relative to that of the pristine nanotube, with the extent of the effect linearly related to the density of oxygen uptake of the SWNT. In the model nanotube system used, the HOMO energy decreases by approximately 50 meV per weight percentage of O_2 in the system. As oxygen binds to the

SWNT, this lowering of the Fermi level (previously inferred from thermopower measurements)[4] reduces the electron donating ability of the nanotube, resulting in the lack of instantaneous reduction of POMs on contact with SWNT in solution and less effective filling of POMs into nanotube *via* the charge transfer process.

Computational methods

The HOMO energy was calculated for each of the ground state species of zero to four di-oxygen molecules chemisorbed to the 1.3 nm long model (8,8) SWNT structure shown in Figure S12, with hydrogen atoms terminating unsaturated edge carbon atoms. Geometry optimizations were performed using the Q-Chem 5.0 quantum chemistry software package[6] at the B3LYP/6-31G* level of theory,[7,8] with structures and energies confirmed using ωB97X-D/6-311G**.[9]

References and Notes

1. C. R. Graham, R. G. Finke, *Inorg. Chem.* **2008**, *47*, 3679.

2. M. Misono, N. Mizuno, K. Katamura, A. Kasai, Y. Konishi, K. Sakata, T. Okuhara, Y. Yoneda, *Bull. Chem. Soc. Jpn.* **1982**, *55*, 400.

3. M. Sadakane, E. Steckhan, *Chem. Rev.* **1998**, *98*, 219.

4. G. U. Sumanasekera, C. K. W. Adu, S. Fang, and P. C. Eklund, *Phys. Rev. Lett.* **2000**, *85*, 1096.

5. D. C. Sorescu, K. D. Jordan, and P. Avouris, *J. Phys. Chem. B* **2001**, *105*, 227.

6. Y. Shao, *et al., Mol. Phys.*, **2015**, *113*, 184.

7. A. D. Becke, *J. Chem. Phys.* **1993**, *98*, 5648.

8. P. J. Stephens, F. J. Devlin, C. F. Chabolowski, and M. J. Frisch, J. Phys. Chem. 98, 11623 (1994).

9. J.-D. Chai and M. Head-Gordon, *Phys. Chem. Chem. Phys.* **2008**, *10*, 6615.